This document is the accepted manuscript version of the following article:

Dachraoui, W., & Erni, R. (2022). Nonclassical nucleation and growth of Pd nanocrystals from aqueous solution studied by in situ liquid transmission electron microscopy. Chemistry of Materials. https://doi.org/10.1021/acs.chemmater.2c03226

Non-Classical Nucleation-and-Growth of Pd Nanocrystals from Aqueous Solution Studied by In-Situ Liquid Transmission Electron Microscopy

Walid Dachraoui[1], Rolf Erni[1]

[1]Electron Microscopy Center, Empa—Swiss Federal Laboratories for Materials Science and Technology, Überlandstrasse 129, CH-8600, Dübendorf, Switzerland.

*Correspondence to:
E-mail: walid.dachraoui@empa.ch
E-mail: rolf.erni@empa.ch

ABSTRACT

Direct visualization and understanding of the atomic mechanisms governing the growth of nanomaterials is crucial for designing synthesis strategies of high specificity. Aside from playing a key role in numerous technological applications, palladium clusters and nanoparticles are particularly valuable due to their outstanding catalytic activity. Studies show that the properties of Pd nanomaterials depend on shape and size. Therefore, optimizing the synthesis to control the final size and shape of Pd nanoparticles is important for a large number of current and future applications. In this work we exploit in-situ liquid cell scanning transmission electron microscopy to track at the atomic scale the growth of Pd nanoparticles form the very early stage to mature, crystalline nanoparticles. We find that the formation of Pd nanoparticles consists of multiple steps. The first step in nanoparticle formation, representing a non-classical nucleation step, can be described by the formation of agglomerates of Pd atoms. In the second step, these agglomerates grow via atomic addition to form primary nanoclusters which coalescence to form amorphous clusters. In the third stage, these clusters continue to coalescence leading to the formation of amorphous Pd NPs, while in parallel growth by monomer attachment continues. Then, in the fourth step, the amorphous nanoparticles undergo a nanocrystallization process where the continuous improvement of crystallinity and the establishment of a distinct morphology eventually give rise to the formation of facetted, crystalline nanoparticles. Similar to our earlier work with Au and Pt nanoparticles, these results confirm that even for simple systems non-classical nucleation and growth processes dominate, and that these multi-step mechanisms are highly element specific. Despite the fact that the synthesis conditions are identical, the element specific interactions define the pathway of the formation of crystalline nanoparticles.

Keywords Nucleation, growth, nanoparticles, Palladium, in situ liquid, TEM

Introduction

Similar to other noble metals like gold and platinum, palladium nanoparticles (NPs) have unique chemical and physical properties, which differ from those of the corresponding bulk material. Sub-10 nm NPs are well-known catalysts for hydrogenation [1, 2] as well as oxidation reactions.[3, 4] The particles' catalytic activity and selectivity significantly depend on particle size[5] and shape.[6] Thus, knowledge about the intermediate products during nucleation and growth is of great importance to control the desired size and shape of NPs and thus to outline an optimal synthesis strategy for producing specific NPs. In literature, only few syntheses of Pd NPs are described which commonly rely on the use of surface modification, stabilizing agents in particular.[7] In addition, the syntheses are often carried out in organic solvents that are unfavorable for applications.[7, 8] Moreover, surface modifications can decrease the catalytic activity of NPs by blocking their active sites which might also be most attractive for these surface agents. Consequently, reliable protocols for Pd NP syntheses in aqueous solution without any stabilizing agent are in high demand.[9] The NPs free of organic stabilizers or ligands ("pristine NPs") can be used directly for catalysis both in aqueous solution and on solid supports. Yet, reliable protocols for the synthesis of Pd NPs in aqueous solution are rarely found, which might indicate that the actual formation mechanism in aqueous solution is complex and does not follow a classical nucleation-and-growth reaction. Understanding the exact atomic mechanism of Pd NPs growth could thus enable the design of reliable protocols for engineering pristine sub-10 nm Pd NPs in aqueous solution.

Descriptions of particle-growth reactions often rely on the classical nanoparticle growth model by LaMer (from 1950s) which is based on the classical nucleation theory developed by Becker and Döring in the 1930s.[10, 11] Although valuable, recent experimental studies, including our own works, have provided clear evidence that the classical nucleation theory and its translation to nanoparticles are insufficient to explain the complex reactions observed.[12-19] There is thus consensus that reliable experimental information at high temporal and spatial resolution is needed in order to uncover the fundamental principles that govern the nucleation and growth of nanoparticles.

Microfabrication-based technologies allowed transmission electron microscopy to overcome limits imposed by vacuum and provide new opportunities for imaging particles in a liquid environment[20-24]. While commercial liquid cell holders are beneficial for various liquid phase studies in electron microscopy, they do not routinely enable atomic resolution imaging with single atom sensitivity.[25, 26]Alternatively, non-commercial graphene liquid cells (GLCs) provide an opportunity to observe nanoparticles at the true atomic-level, with single atom sensitivity. The employed "graphene" sheets are composed of a few graphitic monolayers with an overall thickness below ~1 nm, allowing for imaging liquid samples and particles therein at the Ångström level.[27] In addition, the impermeability and the mechanical flexibility of graphene enable the entrapment of liquid nanoreactors with minimal risk of leakage to the surrounding vacuum environment of the electron microscope. Moreover, graphene's chemical inertness and electrical conductivity minimize unwanted irradiation effects that could interfere with the chemical reactions, which are controlled by the electron beam and intended to be monitored.[28-30]

Our previous in-situ studies of the growth mechanisms of Pt[30], Au[26] and binary Pt-Pd NPs already revealed unexpected element-specific atomic pathways when crystalline nanoparticles are formed. The aim of the present work is to apply the previously optimized methodology of time-resolved in-situ studies by scanning transmission electron microscopy (STEM) of Au-NPS and Pt-NPs to another metallic system, namely, palladium nanoparticles (Pd-NPs), in order to identify common trends in the aqueous-based synthesis of these rather simple metallic particles. The results are then discussed in the context of the widely referenced model of LaMer. And as such, this work challenges the hypothesis of a classical nucleation-and-growth process underlying the formation of monatomic nanoparticles.

Experimental

We used a 5 mM aqueous solution of $Na_2PdCl_4 \bullet 2H_2O$ to study nucleation and growth of Pd nanoparticles. The illumination of water by a high-energy electron beam, 300 kV in our case, can generate a set of well-established primary products[31], namely hydrated electrons (e_h^-), hydrogen radicals ($H^\bullet$), hydroxyl radicals ($HO^\bullet$), hydrogen peroxide (H_2O_2), hydronium ions (H_3O^+), hydroperoxyl radicals ($HO_2^\bullet$), and hydrogen (H_2). Strong reducing agents, such as e_h^- and $H^\bullet$, react with the complex ions of the Pd precursor at diffusion controlled rates. Uniformly distributed within the irradiated area, these reactive species reduce the Pd ions to zerovalent metal atoms and labile atomic clusters.[32] This indirect reduction of the encapsulated Pd precursor by the electron beam thus triggers the formation of Pd nanoparticles, once the Pd concentration exceeds the solubility limit. We should keep in consideration that the radiochemistry in the solution might be affected by the local change in temperature induced by electron beam heating.[33-36]. Despite the fact that we cannot measure the temperature inside the graphene-based nanoreactors, we conclude that the temperature increase in these liquid pocket is moderate and that it is the radiochemistry of the electron beam that governs the observed reaction, because the aqueous solvent remains liquid and does not form gaseous pockets. Moreover, the graphene windows and the small volume warrant that possible heat can be dissipated quickly, particularly when considering the scanning mode of imaging, which does not stationary illuminate the entire field of view as this is the case in the broad beam transmission electron microscopy (TEM) mode.

The time $t = 0$ s in the movies and in Figures represents the starting point of imaging in that particular area, while the preceding optimization of the imaging conditions is done in a different area in order to minimize unwanted beam effects in the area of observation. The electron dose (i.e. $4.2\ 10^3$ electrons/Å^{2}s) and the imaging conditions were optimized to enable the growth of Pd nanoparticles with kinetics suitable to track the nucleation without altering the structures under observation.

Results

Figure 1 shows a sequence of annular dark-field (ADF) STEM images depicting the growth of Pd nanoparticles (see movie S1 for more details). In the beginning, while the electron beam indirectly reduces the Pd precursor, many small nanoclusters are formed. After this initial step, the growth is dominated by nanoclusters interacting with each other to form nanoparticles with different shapes and sizes (see Figure S2 for more details). As shown in Figure 1b, at the end of the growth, distinct single crystalline nanoparticles with a size of around 5 nm are present (see Figure 1b). High-resolution ADF-STEM images and the analysis of their Fourier transforms (FT) show the presence of face-centered cubic (fcc) Pd nanocrystals with a high degree of crystallinity and a lattice constant of about 0.39 nm, similar to the bulk value of Pd[37]. Figure 1c presents the size and number of nanoclusters in the field of view as a function of time (red and blue successively). During the first growth stage, the number of nanoclusters gradually increases and reaches its maximum at ~33 s, after which, suddenly, the number of nanoclusters drops significantly whereas the average particle size increases from less than 1 nm to more than 4 nm. Therefore, at about ~45 s the growth process enters a second growth stage, where the sudden decrease in the number of particles and the correlated increase in particle size is mainly due to the coalescence of individual nanoparticles. The diagram in Fig. 1c depicting the number

of particles in the field of view is divided into three slots highlighted with different colors, where at the beginning the number of nanoclusters increase until the maximum is reached after ~32 s. Thereafter, the number of nanoclusters decreases slowly between 32 and 45 s, which can be related to a first coalescence process to form bigger nanoclusters. Finally, a sharp decrease in the number of nanoparticles can be observed corresponding to a second coalescence process. These different steps clearly indicate that the formation of these Pd NPs is a multi-step growth process governed, as explained below, by coalescence.

In the subsequent part of the manuscript, we will consider ultra-small nanoclusters the (primary) nanoclusters of size below 0.5 nm and bigger nanoclusters for the (secondary) clusters below 1.5 nm, while nanoparticles are considered to exceed 1.5 nm in diameter.

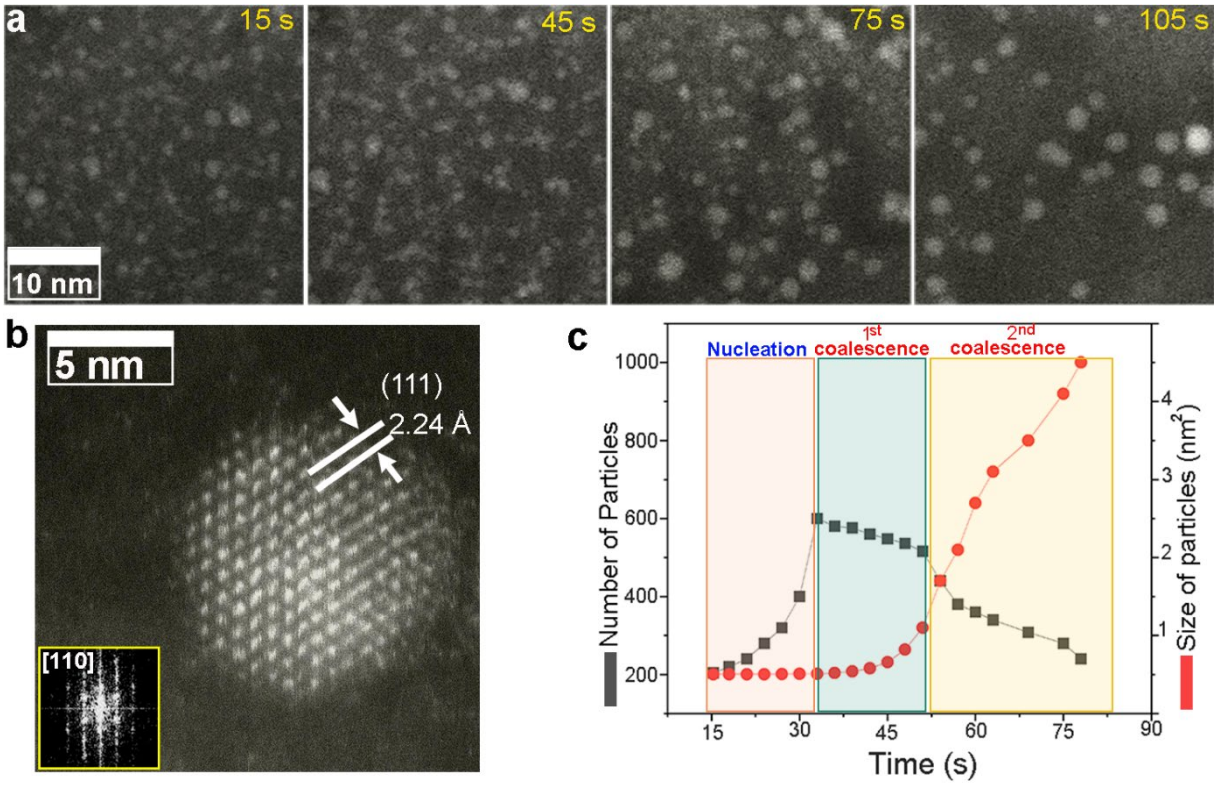

Figure 1: The growth of Pd nanoparticles in a GLC during exposure to the electron beam. **a**. Sequential ADF-STEM images showing the real-time growth of Pd nanoparticles via nanoparticle attachment. **b**. High-resolution ADF-STEM image of a nanoparticle formed during complete growth with corresponding FT pattern. **c**. Average particles size evolution (red) and the number of particles (blue) as a function of time. Images are shown in false colour.

Although Fig. 1a and the analysis in Fig. 1c provide evidence for different steps, they do not provide information about the atomic mechanisms that control particle formation due to the limit in terms of resolution related to general view of the growth. In order to identify these atomic mechanisms of the formation of Pd NPs, we first examined the initial step where individual Pd atoms are present and their transition into aggregates of diameters less than 0.5 nm, using high-resolution ADF-STEM images with a temporal resolution of 2 frames per second. Figure 2a shows sequential atomic-resolution snapshots depicting the nucleation of rather lose Pd aggregates in the imaged area. The bright dots in Fig. 2a correspond to Pd atoms, which after 9 s of illumination start to form the above mentioned aggregates (highlighted with dashed white lines). Then, the formed aggregates appear to act as seeds for the atoms in the surrounding liquid area, which rapidly attach

to form ultra-small nanoclusters, which we refer to as primary nanoclusters. The primary nanoclusters continue growing by single atom attachment. Figure 2b shows a schematic illustration of this non-classical nucleation and the formation of primary Pd nanoclusters.

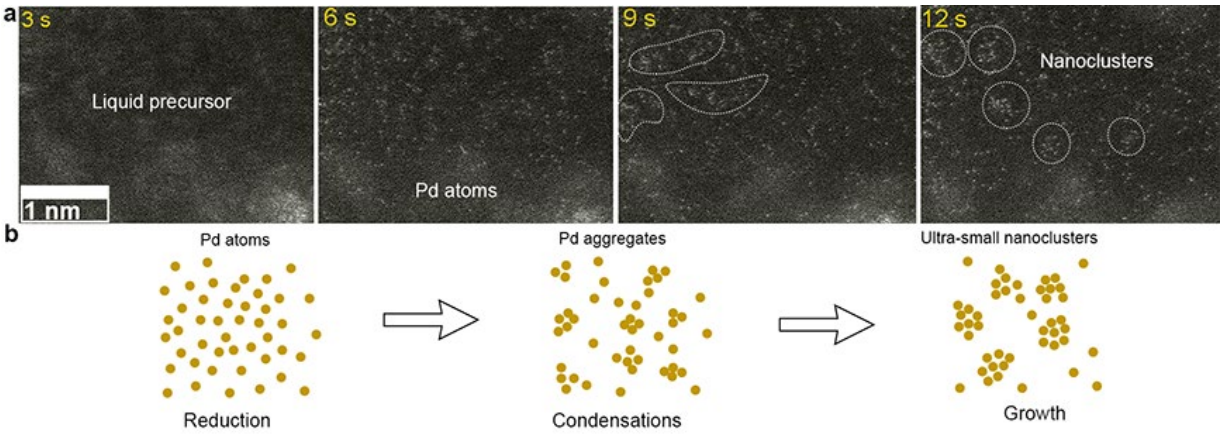

Figure 2: Nucleation and growth of ultra-small nanoclusters. **a**. Image sequences from movie S2 showing the nucleation and growth of Pd nanoclusters, where atoms migrate through the liquid to attach to each other to form aggregates. At the end of the series, a set of ultra-small nanoclusters less than 1 nm in size are formed. **b**. Schematic illustration of the nucleation and growth of nanoclusters. Images are shown in false colour.

In the second step, primary nanoclusters (< 0.5nm) are involved in a coalescence process to form bigger nanoclusters, which is documented in Fig. 3a (see movie S3 for details), where two groups of nanoclusters are highlighted. In the red rectangle three ultra-small nanoclusters less than 0.5 nm are present. The time-resolved high-resolution ADF-STEM images in Figure 3a show that a pair of nanoclusters, formed during the first growth stage undergo a coalescence process. Here, during the whole process the two nanoclusters are in the same focus, which allows us for considering the projected distance between them as the real separation distance. Initially, both nanoclusters of s about 0.2 nm diameter are separated by about 0.3 nm at t = 5 s. Then, both nanoclusters in the solution start to continuously move and rotate in an apparently random fashion, while slowly approaching and then move away from each other (see Movie S3 for details). When they finally get closer, to a distance of about 0.2 nm at t = 15 s, these nanoclusters start to interact to form a bigger nanocluster. Initially, at 25 s two nanoclusters approach and form a nanobridge, marked by the black arrow in Fig. 3a. The thickness of this nanobridge increases until the nanoclusters completely merge at 40 s to form a bigger nanocluster. This coalescence is followed by an attachment of the third nanocluster. In the second example (green rectangle), four primary nanoclusters undergo coalescence to form a larger cluster whose structure can still be explained as being amorphous. These experimental observations are summarized in the schematic representation in Fig. 3b, where the primary nanoclusters are shown to undergo coalescence mostly bridge-induced.[38] The nanoparticles formed during these early stages continue to move and float in the liquid, with no apparent crystallinity. In addition, more primary nanoclusters emerge during the ongoing coalescence processes to form these secondary nanoclusters (see Figure S3 for details).

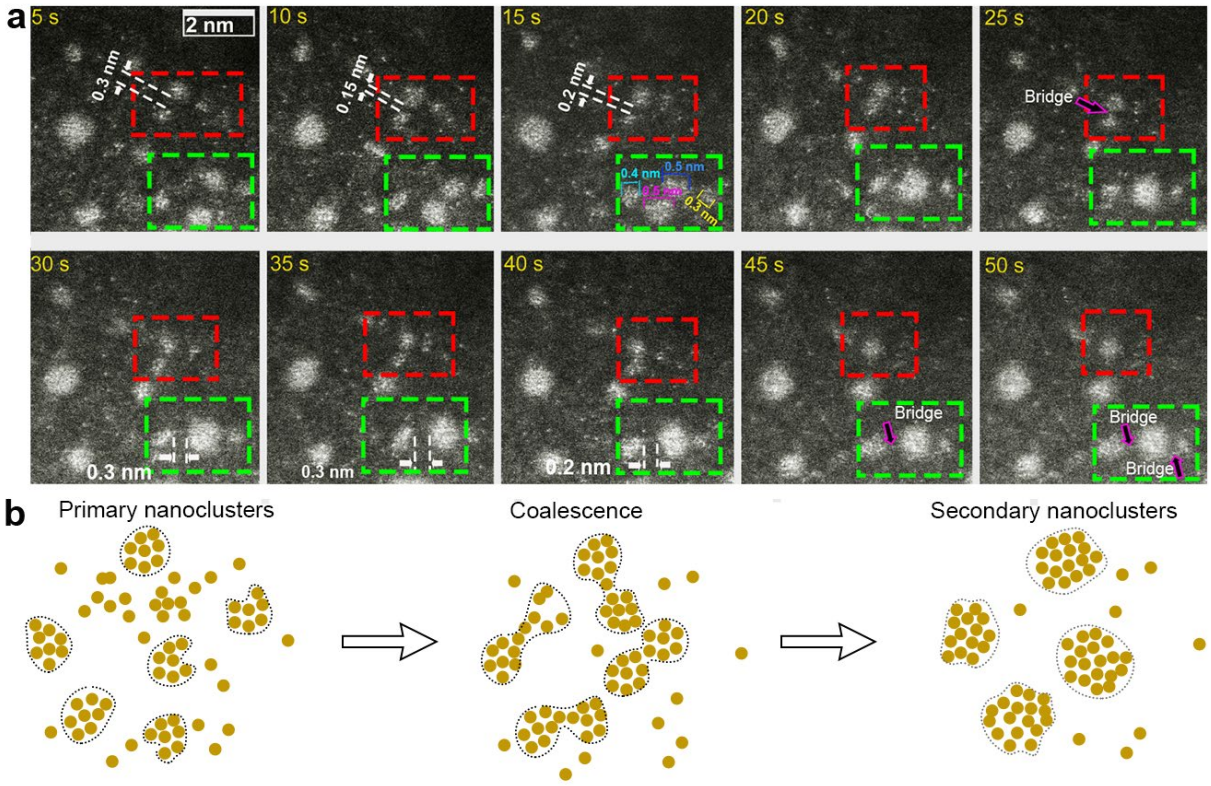

Figure 3: Growth of Pd nanoparticles from aqueous solution under electron beam illumination via nanocluster attachment. **a**. Time-lapse series of atomic-resolution ADF-STEM images showing the growth of Pd nanoparticles via nanoclusters coalescence. **b**. Schematic illustration of the growth of Pd nanoparticles via nanoclusters coalescence. Images are shown in false colour.

Under the influence of the electron beam, the secondary nanoclusters were observed to further grow and coalesce. Figure 4 shows a sequence of frames from movie S4 showing the coalescence dynamics of primary nanoclusters with sizes less than 1 nm undergoing a first coalescence process to generate secondary nanoclusters, which are involved in a second coalescence process to form amorphous nanoparticles. While the primary and secondary nanoclusters' surface is not well defined, the resulting, larger amorphous nanoclusters exhibit well-defined shapes and surfaces, and thus can be classified as nanoparticles. The exact process of this secondary coalescence process is depicted in the schematic illustration of Fig. 4 (more details can be found in movie S4). Figure 4b reveals another mechanism of particle coalescence in this second step, where the clusters approach and form an ultra-thin bridge, indicated by the green arrow in Fig. 4b (more details can be found in movie S5). The bridge broadens over time until the nanoclusters merge to form a bigger nanoparticle after 175 s. Please note, primary nanoclusters in the surrounding area are observed to attach to the bigger ones involved in the coalescence process.

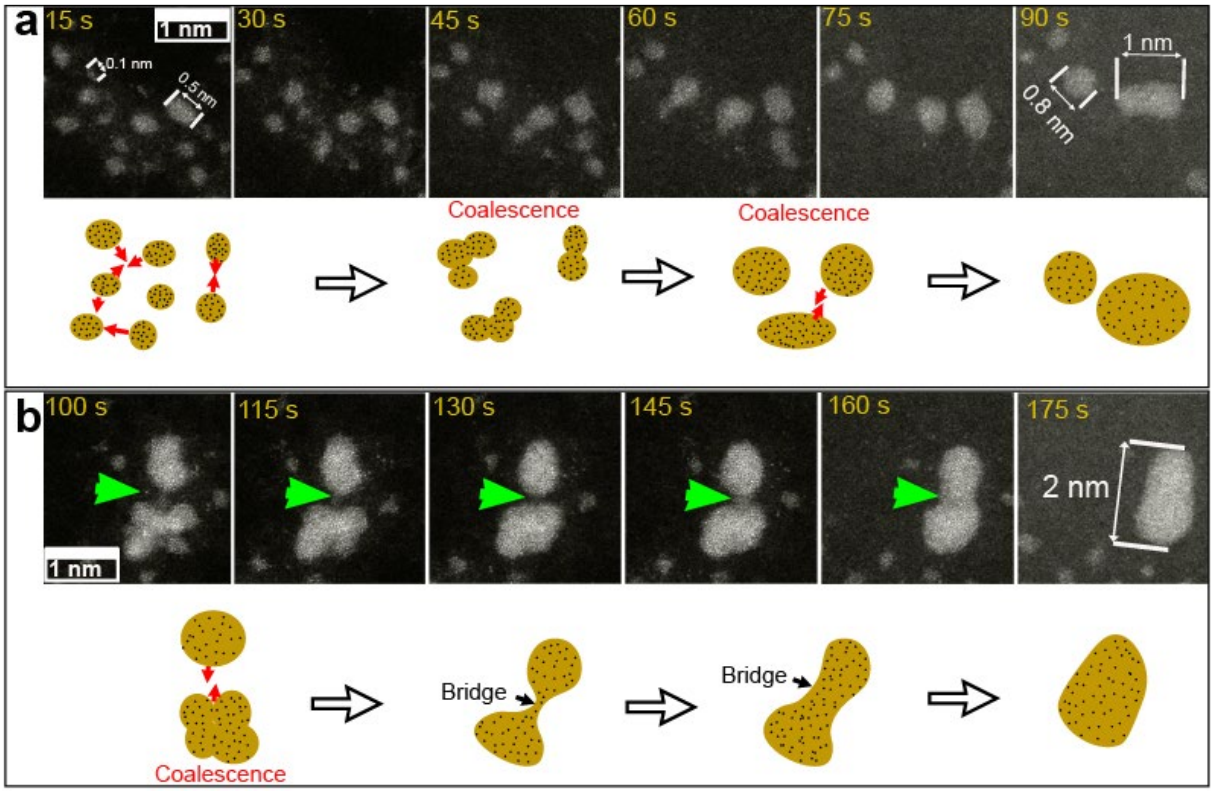

Figure 4: Growth of Pd nanoparticles via coalescence from aqueous solution under electron beam illumination. (**a**) Top: Time-lapse series of atomic-resolution HAADF-STEM images showing a group of ultra-small-nanoclusters less than 1 nm in size undergoing coalescence to form amorphous nanoparticles. Bottom: the corresponding schematic illustration. (**b**) Top: Time-lapse series of atomic-resolution HAADF-STEM images showing a group of ultra- nanoclusters around 1 nm in size undergoing coalescence to form amorphous nanoparticles. Bottom: the corresponding schematic illustration. Images are shown in false colour.

After these two coalescence processes, initially from primary clusters to secondary clusters and then to amorphous nanoparticles, these amorphous nanoparticles exceeding ~1 nm in size undergo nanocrystallization and reshaping where the Pd NP transform to a crystalline state and change from a roundish shape to a distinct facetted morphology. Figure 5 documents this nanocrystallization mechanism in a series of images taken from movie S6. Figure 5a highlights sequential high-resolution ADF-STEM images that depict the coalescence of two amorphous nanoclusters to form an amorphous nanoparticle which undergoes nanocrystallization and related reshaping. Please notice, that due to the coalescence of two nanoclusters a twin boundary is observed in Fig. 5b, which, as part of a ripening process, is eliminated at the end of the crystallization step. Moreover, after 200 s the crystalline nanocrystal starts to change its shape, from a roundish shape to a facetted morphology (designed by yellow dashed lines). This observation can be explained by the fact that the surface energy of the amorphous particle is isotropic, enabling a roundish particle shape, while the crystalline particle favors crystalline planes of low surface energy, leading to the facetted morphology.

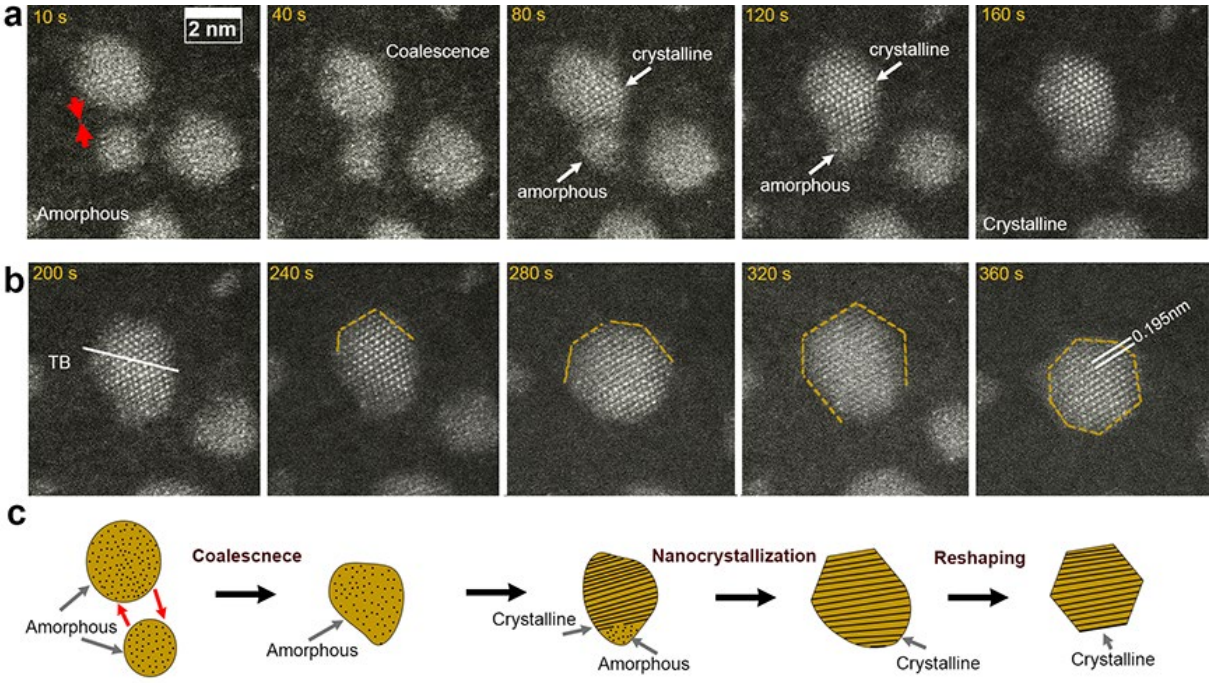

Figure 5: Nanocrystallization and reshaping of Pd nanoparticle. Top: **a** and **b**. Time-lapse series of atomic-resolution HAADF-STEM images shows transition of one amorphous nanoparticle formed via coalescence to crystalline phase and reshaping. **c**. The corresponding schematic illustration. Images are shown in false colour.

Discussion and Conclusions

Our observations of the formation of Pd nanoparticles can be summarized as follows. In a first step aggregates of Pd atoms are formed which act as seeds for Pd atoms to attach and form primary Pd nanoclusters. These primary nanoclusters undergo coalescence to form secondary, still amorphous nanoclusters. In the second coalescence process, the secondary nanoclusters undergo, mostly bridge-induced, coalescence to form roundish and amorphous nanoparticles with well-defined surfaces. These amorphous nanoparticles eventually become crystalline, which also leads to the formation of pronounced facets, defining the morphology of the formed Pd nanocrystals. Figure 6 schematically summarizes the entire growth mechanism of Pd nanoparticles as we observed it in the graphene liquid cell. While our observations allow us to document the diversity, the complexity and dynamics of nanoparticle growth processes in liquid, uncovering the atomic mechanisms controlling and triggering particle growth, it needs to be distinguished from the study made by Cao *et al*, for example, where at the atomic level particle growth is investigated that occurs heavily confined in single-walled carbon nanotubes.[39] Moreover, our work confirms mechanisms suggested by theory, while linking classical and non-classical aspects of the corresponding theories. Indeed, our results support the work by Polte and co-workers about the mechanism of Pd nanoparticle growth where they found that after formation of Pd atom clusters, metastable particles emerge and finally stable nanoparticles, both via coalescence.[40] Yet, our study goes beyond that work as it also uncovers the intermediate processes and products such as the formation of aggregates as the trigger of the reaction and it provides information about the (non-)crystallinity of the clusters after the first and second step.

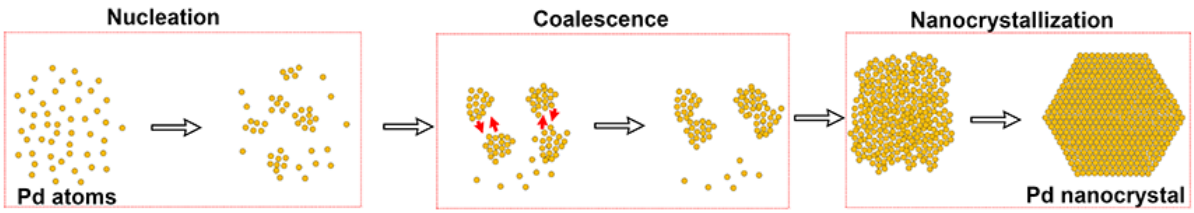

Figure 6: Schematic illustration of the deduced growth mechanism of Pd nanoparticles from in situ GLC observations.

With the results presented we now can come back to LaMer's model for the growth of nanoparticles and discuss its applicability for the system investigated here. In LaMer's model nucleation is instantaneous, at the very beginning of the reaction when solute concentration reaches a critical value.[10] Thereafter the number of nuclei and final particles is set. This is clearly in contradiction to our experiments where we see a continuous formation of nuclei and even during the growth process of nanoclusters and nanoparticles further nucleation events can be observed. This discrepancy could be explained by the fact that during electron irradiation additional Pt ions are being reduced thus leading to reach locally critical concentrations such that additional nucleation events occurs. In respect to the rather small liquid volume we probe by the electron beam and considering the overall reactive environment formed during nearly continuous electron irradiation, this explanation does not seem to be appropriate. Hence, based on our observation, it seems more likely that an instantaneous nucleation event is not a realistic description of a nucleation reaction, at least for the system investigated here and for the systems we investigated in the recent past.[25, 30,41] Moreover, in LaMer's model the number of nuclei reflects the number of formed nanoparticles. Another aspect, where our experimental data contradicts LaMer's model concerns the growth of the clusters and nanoparticles. This aspect is more important as the instantaneous nucleation does not refer to an actual process, except for the statement that suddenly a certain number of nuclei start growing. When it comes to particle growth we can compare the suggested process with the actually observed one. In LaMer's model, particle growth occurs solely via diffusion-controlled addition of single atoms (or single molecules), but particle interaction, coalescence and aggregation do not occur. In our experiments, we clearly see that coalescence and particle interactions are the driving mechanism for particle growth, particularly during the early stages. This also explains the decrease of the number of particles with increasing time (see Fig. 1c), whereas in LaMer's model the number of particles is constant throughout the entire particle formation process and given by the number of nuclei formed at the start. Hence, despite of its popularity, LaMer's model, involving two steps, namely sudden nucleation followed by particle growth, does not seem to be an adequate approach to describe the rather complex nucleation-and-growth reactions that we observe for the case of Pd. Nucleation appears to be an ongoing process that accompanies particle growth, and particle agglomeration and coalescence are important mechanisms for the growth of the Pd nanoparticles. Also the fact that particles undergo a crystallization step is an aspect that cannot be related to LaMer's model. As already pointed out in literature (see, e.g., [42]), the simplicity of LaMer's model, though attractive, is difficult to relate to realistic systems, because of its far-reaching approximations.

It is not the goal of the present experimental study to derive a theoretical model for particle nucleation and growth, but based on the results presented, we can suggest aspects that such an improved model would need to encompass; (i) nuclei appear to form through a local condensation of lose clouds of individual atoms by local concentration fluctuations (Fig. 2a), (ii) continuous nucleation events with (sub-critical) nuclei forming and dissolving, (iii) multiple ways of particle growth; by single atom attachment, by attachment of small clusters as well as by particle coalescence and agglomeration, (iv) a statistical variation of the local environment of the growing particles, as the local environment seems to control the local growth pathway of a selected particle or cluster, (v) an increase of the mean inter-particle distance and thus a gradual change of growth mode with time: from dominant particle agglomeration towards diffusion-controlled single atom attachment until growth stops when the solution is depleted; and finally (vi) in the case of Pd, the early clusters and particles are amorphous and only adopt the bulk crystalline structure in a later stage, when particles reach a size larger than about 1 nm. As we clearly see differences in particle nucleation and growth for different elements and alloys (Au, Pt, Pt-Pd, Pd), some of these aspects are likely dependent on the actual element or system. Nevertheless, the variety of interactions that a generally applicable model would need to encompass shows that such a model is of high complexity and requires addressing element-specific atom-atom interactions and not just bulk properties translated to small volumes with large relative surfaces and whose atomic structure might deviate from the bulk crystalline structure.

In summary, the present study emphasizes that particle growth processes are more complex than captured by classical theory. Moreover, comparing the present results with our previous studies on Au and Pt particles highlights that particle nucleation-and-growth processes are highly element specific. Overall, the present work shows that Pd nanocrystals can form from supersaturated aqueous solution via a four-step mechanism: decomposition, solidification, coalescence and nanocrystallization. Up to now, little success has been achieved in controlling the shape and size of pure noble sub-5nm Pd nanoparticles during the synthesis in aqueous solution. The results presented here, which reveal the underlying atomic mechanisms governing the growth of Pd NPs in aqueous solution, will be of high importance to better control the synthesis of well defined Pd nanoparticles.

ASSOCIATED CONTENT

Supporting Information

Details for the sample preparation, GLCs fabrication, methods for analyses, and Figures S1-S5 (PDF).

In-situ HAADF-STEM observation of Pd nanoparticle growth in aqueous solution under electron beam irradiation(AVI), In-situ HAADF-STEM observation of the reduction of Pd precursor with electron beam (AVI), In-situ HAADF-STEM observation at atomic level of few Pd ultra-small nanoclusters undergoing a coalescence process (AVI). In-situ HAADF-STEM observation at atomic level of a pair of Pd amorphous nanoclusters undergoing a coalescence process to form bigger nanoclusters (AVI), In-situ HAADF-STEM observation at atomic level of many amorphous nanoclusters of Pd undergoing a coalescence process to form amorphous nanoparticles (AVI). In-situ HAADF-STEM observation at atomic level of a pair of Pd amorphous nanoclusters undergoing a coalescence and nanocrystallization processes (AVI).

AUTHOR INFORMATION

Corresponding Author

*Email**:** walid.dachaoui@empa.ch

*Email**:** rolf.erni@empa.chmailto:

ORCID

Walid Dachraoui: 0000-0001-7599-5856

Authors' Contributions

W.D. conceived the idea and wrote the manuscript. W.D. fabricated the liquid cells, performed the liquid-cell experiments and realised the in-situ STEM characterizations. W.D carried out the data analysis. R.E supervised the project. All authors discussed the results and commented on the manuscript.

Notes

The authors declare no competing interests.

DATA AVAILABILITY

The data that support the findings of this study are available from the corresponding author upon reasonable request

References

1- Zamborini, F. P.; Gross, S. M.; Murray, R. W. Synthesis, Characterization, Reactivity, and Electrochemistry of Palladium Monolayer Protected Clusters. Langmuzir **2001**, 17, 481-488

2- Son, S. U.; Jang, Y.; Yoon, K. Y.; Kang, E.; Hyeon, T. Facile Synthesis of Various Phosphine-Stabilized Monodisperse Palladium Nanoparticles through the Understanding of Coordination Chemistry of the Nanoparticles. Nano Lett **2004**, 6, 1147-1151

3- Andre, R.; de Jesu, E.; Flores, J. C. Catalysts based on palladium dendrimers. New. J. Chem **2007**, 31, 1161-1191.

4- Piao, Y.; Jang, Y.; Shokouhimehr, M.; Lee, I. S.; Hyeon,T. Facile Aqueous-Phase Synthesis of Uniform Palladium Nanoparticles of Various Shapes and Sizes. Small **2007**, 3, 255-260.

5- Narayanan, R.; El-Sayed, M. A. Some Aspects of Colloidal Nanoparticle Stability, Catalytic Activity, and Recycling Potential. Top Catal **2008**, 47. 15-21.

6- Jin, M.; Liu, H.; Zhang, H.; Xie, Z.; Liu, J.; Xia, Y. Synthesis of Pd Nanocrystals Enclosed by {100} Facets and with Sizes <10 nm for Application in CO Oxidation. Nano Res **2011**, 4, 83-91.

7- Yuan, Q.; Zhuanga, J.; Wang, X. Single-phase aqueous approach toward Pd sub-10 nm nanocubes and Pd–Pt heterostructured ultrathin nanowires. Chem comm **2009**, 6613-6615.

8- Lim, B. B.; Jiang, M.; Tao, J.; Camargo, P. H. C., Yimei Zhu,andYounan Xia. Shape-Controlled Synthesis of Pd Nanocrystals in Aqueous Solutions. Adv. Funct. Mater **2009**, 19, 189-200.
9- Ikeda, S.; Ishino, S.; Harada, T.; Okamoto, N.; Sakata, T.; Mori, H.; Kuwabata, S.; Torimoto, T.; Matsumura, M. Ligand-Free Platinum Nanoparticles Encapsulated in a Hollow Porous Carbon Shell as a Highly Active Heterogeneous Hydrogenation Catalyst. Angew. Chem **2006**, 118, 7221-7224.
10- LaMer, V. K.; Dingegar, R. H. Theory, Production and mechanism of Formation of Monodispersed Hydrosols.Journal of the American Chemical Society **1950**, 72, 4847-4854.
11- Becker, R.; D¨oring, W. Kinetische behandlung der Keimbildung in ubersattigten dampfern. Annalen der Physik **1935**, 24, 719.
12- Einstein, A.; Podolsky, B.; Rosen, N. Can quantum-mechanical description of physical reality be considered complete? Phys. Rev **1935**, 47, 777-780.
13- Sugimoto, T.; Shiba, F. Spontaneous nucleation of monodisperse silver halide particles from homogeneous gelatin solution II: silver bromide. A: Physicochem. Eng. Aspects **2000**, 164, 205-215.
14- Zheng, H.; Smith, R. K.; Jun, Y. W.; Kisielowski, C.; Dahmen, U.; Alivisatos, A. P. Observation of Single Colloidal Platinum Nanocrystal Growth Trajectories. Science **2009**, 324, 1309-1312.
15- Liao, H. G.; Likun, C.; Stephen, W.; Haimei, Z. Real-Time Imaging of Pt_3Fe Nanorod Growth in Solution. Science **2012**, 336, 1011-1014.
16- Dae, K. S.; Chang, J. H.; Koo, K.; Park, J., Kim, J. S. & Yuk, J. M. Real-Time Observation of $CaCO_3$ Mineralization in Highly Supersaturated Graphene Liquid Cells. ACS Omega **2020**, 5, 14619-14624.
17- Jeon, S.; Heo, T.; Hwang, SY.; Ciston, J.; Bustillo, K. C.; Reed, B. W; Ham, J.; Kang, S.; Kim, S.; Lim, J.; Lim, K.; Kim, J. S.; Kang, M. H.; Bloom, R. S.; Hong, S.; Kim, K.; Zettl, A; Kim, W. Y.; Ercius, P.; Park, J.; Lee, W. C. Reversible disorder-order transitions in atomic crystal nucleation. Science **2021**, 29, 498-503.
18- Nielsen, M. H.; Aloni, S.; De Yoreo, J. J. In situ TEM imaging of $CaCO_3$ nucleation reveals coexistence of direct and indirect pathways. Science **2014**, 5, 1158-62.
19- Loh, N. D.; Sen, S.; Bosman, M.; Tan, S. F.; Zhong, J.; Nijhuis, C. A.; Král, P.; Matsudaira, P.; Mirsaidov, U. Multistep nucleation of nanocrystals in aqueous solution. Nat Chem **2017**, 9, 77-82.
20- Song, B.; He, K.; Yuan, Y.; Sharifi-Asl, S.; Cheng, M.; Lu, J.; Saidi, W. A.; Shahbazian-Yassar, R. In situ study of nucleation and growth dynamics of Au nanoparticles on MoS2 nanoflakes. Nanoscale **2018,** 10, 15809-15815.
21- Junjie, L.; Jiangchun, C.; Wang, H.; Na, C.; Wang, Z.; Guo, L.; Deepak, F. L. In situ atomic-scale study of particle-mediated nucleation and growth in amorphous bismuth to nanocrystal phase transformation. Adv. Sci **2018,** 5, 1700992.
22- Wand, M.; Park, C.; Woehl, T. J. Quantifying the Nucleation and Growth Kinetics of Electron Beam Nanochemistry with Liquid Cell Scanning Transmission Electron Microscopy. Chem. Mater Chem. Mater **2018**, 30, 7727-7736.
23- Nielsen, M. H.; Li, D.; Zhang, H.; Aloni, S.; Han, T. Y. J.; Frandsen, C.; Seto, J.; Banfield, J. F.; Cölfen, H.; De Yoreo, J. J. Investigating Processes of Nanocrystal Formation and Transformation via Liquid Cell TEM. Microsc. Microanal **2014,** 20, 425-436.
24- Wie, W.; Zhang, H.; Wang, W.; Dong, M.; Nie, M.; Sun, L.; Xu, F. Observing the Growth of Pb_3O_4 Nanocrystals by in Situ Liquid Cell Transmission Electron Microscopy. ACS Appl. Mater. Interfaces **2019,** 11, 24478-24484.
25- Dachraoui, W.; Keller, D.; Henninen, T. R.; Ashton, O. J.; Erni, R. Atomic Mechanisms of Nanocrystallization via Cluster-Clouds in Solution Studied by Liquid-Phase Scanning Transmission Electron Microscopy. Nano Lett **2021,** 21, 2861-2869.
26- Zhang, Y.; Keller, D.; Rossell, M. D.; Erni, R. Formation of Au nanoparticles in liquid cell transmission electron microscopy: from a systematic study to engineered nanostructures, Chemistry of Materials **2017**, 29 10518-10525
27- Wang, C.; Shokuhfar, T.; Klie, R.F. Precise In Situ Modulation of Local Liquid Chemistry via Electron Irradiation in Nanoreactors Based on Graphene Liquid Cells Adv. Mater **2016,** 28, 7716-7722.
28- Wang, C.; Shokuhfar, T.; Klie, R.F. Precise In Situ Modulation of Local Liquid Chemistry via Electron Irradiation in Nanoreactors Based on Graphene Liquid Cells Adv. Mater **2016**, 28, 7716-7722.
29- Dachraoui, W.; Bodnarchuk, M. I.; Vogel, A.; Kovalenko, M. V; Erni, R. Unraveling the shell growth pathways of Pd-Pt core-shell nanocubes at atomic level in situ liquid cell electron microscopy. Appl. Phsy. Rev **2021,** 08, 041407.
30- Dachraoui, W.; Henninen, T. R.; Keller, D.; Erni, R. Multi-Step Atomic Mechanism of Platinum Nanocrystals Nucleation and Growth Revealed by In-Situ Liquid Cell STEM Scientific Reports **2021,** 11, 23965.
31- Schneiderm, N. M.; Norton, M. M.; Mendel, B. J.; Grogan, J. M.; Ross, F. M.; Bau, H. H. Electron−Water Interactions and Implications for Liquid Cell Electron. J. Phys. Chem. C **2014**, 118, 22373−22382
32- Harold, A. S. Free Radicals Generated by Radiolysis of Aqueous Solutions. Journal of Chemical Education **1981,** 58, 101-105.
33- Hsieh, T. H.; Chen, J. Y.; Huang, C. W.; Wu, W.W. Observing Growth of Nanostructured ZnO in Liquid. Chem. Mat **2016**, 28, 4507-4511.

34- Fritsch, B.; Hutzler, A.; Wu, M.; Khadivianazar, S.; Vogl, L.; Jank, M. P.M.; März, M. Spiecker, E. Accessing local electron-beam induced temperature changes during in situ liquid-phase transmission electron microscopy. Nanoscale Adv **2021**, 3, 2466-2474.
35- Schäfer, S.; Liang, W.; Zewail, A. H. Structural dynamics of surfaces by ultrafast electron crystallography: Experimental and multiple scattering theory. J. Chem. Phys **2011**, 135, 214201.
36- Fritsch, B.; Zech, T. S..; Bruns, M. P.; Körner. A.; Khadivianazar, S.; Wu, M.; Talebi, N. Z.; Virtanen, S.; Unruh, T.; Jank, M. P.M.; Spiecker, E.; Hutzler, A. Radiolysis-Driven Evolution of Gold Nanostructures –Model Verification by Scale Bridging In Situ Liquid-PhaseTransmission Electron Microscopy and X-Ray Diffraction. Adv. Sci **2022**, 9, 2202803
37- Ikeda, S.; Ishino, S.; Harada, T.; Okamoto, N.; Sakata, T.; Mori, H.; Kuwabata, S.; Torimoto, T.; Matsumura, M. Ligand-Free Platinum Nanoparticles Encapsulated in a Hollow Porous Carbon Shell as a Highly Active Heterogeneous Hydrogenation Catalyst. Angew. Chem **2006**, 118, 7221-7224.
38- Keller, D.; Henninen, T. R.; Erni, R. Atomic mechanisms of gold nanoparticle growth in ionic liquids studied by in situ scanning transmission electron microscopy. Nanoscale 2020, 12, 22511-22517
39- Cao, K.; Biskupek, J.; Stoppiello, C. T.: Mc Sweeney, R. L.; Chamberlain, T. W.; Liu, Z.; Suenaga, K.; Skowron, S.T.; Besley, E.; Khlobystov, A. N.; Kaiser, U. Atomic mechanism of metal crystal nucleus formation in a single-walled carbon nanotube. Nat Chem. **2020**, 10, 921-928.
40- Kettemann, F.; Wuithschick, M.; Caputo, G.; Kraehnert, R.; Pinna, N.; Rademann, K.; Polte, J. Reliable palladium nanoparticle syntheses in aqueous solution: the importance of understanding precursor chemistry and growth mechanism. Cryst Eng Comm **2015**, 17, 1865–1870.
41- Dachraoui, W.; Bodnarchuk, m. I.; Erni, R. Direct Imaginbg of the Atomic Mechanisms Governing the Growth and Shape of Bimetallic Pt-Pd Nanocrystals by In-Situ Liquid Cell STEM. ACS Nano 2022, 16, 14198-14209.
42- Whitehea, C. B. d.; Özkar, S.; Finke, R. G. LaMer's 1950 Model for Particle Formation of Instantaneous Nucleation and Diffusion-Controlled Growth: A Historical Look at the Model's Origins, Assumptions, Equations, and Underlying Sulfur Sol Formation Kinetics Data Chem. Mater **2019**, 31, 7116-7132.